Understanding the Effect of Doping on Energetics and Electronic Structure for Au_{25}, Ag_{25} and Au_{38} Clusters

Fahri Alkan[a], Pratima Pandeya[a] and Christine M. Aikens[a,*]

a) Department of Chemistry, Kansas State University, Manhattan, KS 66506, USA
* cmaikens@ksu.edu; 1-785-532-0954

ABSTRACT

We investigate the doping process theoretically for singly doped MAu_{24}, MAg_{24} and MAu_{37} (M=Ni, Pd, Pt, Cu, Ag/Au, Zn, Cd, Hg, Ga, In and Tl) clusters using density functional theory (DFT). For all clusters, the group X dopants (Ni, Pd and Pt) prefer the central location due to the relative stability of d electrons in the dopant. For dopants in groups XI-XIII, doping on the surface of the core and the ligand shell in MAu_{24} become thermodynamically more preferable as a result of symmetry-dictated coupling between dopant atomic orbitals and super-atomic levels as well as because of relativistic contraction of s and p orbitals. The same mechanisms are also found to be responsible for the relative isomer energies in MAu_{37} clusters. For these clusters, DFT calculations predict that it is unlikely for the dopant atom to occupy the central location. We found similar trends for different dopants across the periodic table in relative isomer energies of MAu_{24} and MAg_{24}; however, center-doped clusters are somewhat more stable in the case of MAg_{24} due to the smaller relativistic stabilization of s and p levels in Ag compared to Au. We also found that the metallic radii of the dopant can affect the geometries and relative stabilities of the isomers for the doped clusters significantly.

INTRODUCTION

Atomically precise thiolate-protected metal (especially gold and silver) nanoparticles have attracted significant research interest due to their distinct electronic and optical properties.[1-8] As a result of these properties, thiolate-protected metal nanoparticles can offer different applications in the areas of catalysis,[9-13] biosensors[14-15] and electronics.[16] The structures of these particles are often composed of a metallic core, which is protected by a ligand shell that consists of M-SR staple units.[5, 17] A large number of different thiolate-protected gold nanoparticles[1, 5, 8, 18-22] and silver nanoparticles[23-25] have been characterized successfully in the last decade. Among these particles, $Au_{25}(SR)_{18}^{-1}$ (Au_{25}^{-1} for short) has attracted the most attention due to its relatively high stability.[26] The structure of Au_{25}^{-1} consists of a nearly icosahedral Au_{13} core surrounded by $Au_2(SR)_3$ staple motifs.[1, 3, 5] The silver analogue of Au_{25}^{-1} cluster, Ag_{25}^{-1}, has also been characterized previously.[24] Another extensively studied thiolate-protected nanocluster is $Au_{38}(SR)_{24}$ (Au_{38} for short), which exhibits an elongated Au_{23} core protected by $Au_2(SR)_3$ staple motifs.[18, 27] Comprehensive structure listings of other gold or silver nanoparticles can be found in several recent reviews.[6-7, 23, 28-29]

The concepts of super-atoms and super-atomic orbitals[30-31] have often been employed to understand the electronic structure, stability and optical properties of thiolate-protected gold and silver nanoparticles.[2, 4-5, 32] In the case of the Au_{25}^{-1} cluster, the super-atom model and electron counting rules predict a $1S^21P^61D^0$ electronic configuration with 8 valance electrons,[4] which is analogous to a noble gas configuration. A similar electronic structure has been shown for the Ag_{25}^{-1} cluster with the same super-atomic electron configuration.[24] The super-atomic model can also give insight into the electronic structure of the $Au_{38}(SR)_{24}$ cluster (Au_{38}), which can be viewed as a super-atomic molecule.[33] In this case, the molecular orbitals of the cluster are analogous to the σ, π, δ… levels of a homonuclear diatomic system.[27, 33]

Doping of thiolate-protected nanoclusters with heteroatoms is an exciting strategy to synthesize new alloys with novel properties. The doping route for Au_{25}^{-1} cluster has been first explored by Murray and coworkers experimentally,[34] and by Jiang et al.[35] and Walter and Moseler[36] using theoretical methods. Since their pioneering work, different foreign metals such as Ag,[37-39] Cu,[38] Cd,[40] Hg,[40] Pd,[41-46] Pt[42, 44-45] and Ir[47] have been incorporated into the Au_{25}^{-1} structure successfully. While the Au_{25}^{-1} cluster is the most extensively studied cluster for doping so far, doped systems for Ag_{25}^{-1} and Au_{38} have also been reported in the literature.[48-56]

An important question for the doped gold or silver nanoclusters is the preferred location of the foreign metal and the resulting structure of the isomers. In the case of Au_{25}^{-1} and Ag_{25}^{-1}, three different locations exist for a single dopant: the center of the Au_{13} or Ag_{13} icosahedron, the shell of the icosahedron, or the ligand shell. The possible dopant sites for the Au_{38} system can also be characterized similarly; however, there are multiple symmetrically inequivalent sites available for the core shell and the ligand shell of this cluster.[53] Structural studies for doped clusters show that the preferred location of the foreign atom depends on the type of dopant.[6, 26, 29] For example, experimental evidence suggests that both Pd and Pt prefer the central location in Au_{25}^{-1} and Ag_{25}^{-1} clusters,[44-45, 48, 50] whereas conflicting reports exist in the literature for the location of Pd in the Au_{38} cluster.[51, 54, 56] In comparison, Ag prefers the core-surface location in both Au_{25}^{-1} and Au_{38} clusters,[37, 53] and Au prefers the central location when doped into the Ag_{25}^{-1} cluster.[49] In other reports, X-ray structural analysis suggests core-surface doping and ligand-shell doping for Cd and Hg dopants respectively for Au_{25}^{-1}.[40, 57]

In a recent study, we have shown that the central position is favored significantly for group IX metals (Co, Rh and Ir) in the Au_{25}^{-1} cluster as a result of interactions between d electrons of the dopant and the super-atomic levels that originate from the Au_{12} core of the cluster.[58] However, the

mechanisms for the preferred location of other dopants such as Ag/Au or Cd are still not clear for Au_{25}^{-1}. Additionally, other nanoclusters beside Au_{25}^{-1} need to be explored in order to extend our understanding of the effects of doping on energetics and electronic structure. In this work, we have employed a detailed DFT study on the doping process of Au_{25}^{-1}, Ag_{25}^{-1} and Au_{38} clusters in order to investigate the mechanism for the preferred location of different dopants. The effect of doping on the electronic structures and the geometries of these nanoclusters are investigated using theoretical tools. The theoretical results of this study along with previously obtained experimental structures of doped nanoclusters can reveal the mechanisms for the preferred location of various dopants in metal-nanocluster chemistry.

COMPUTATIONAL DETAILS

Calculations were performed for the doped clusters of $MAu_{24}(SH)_{18}^{q}$ (abbreviated as MAu_{24}), $MAg_{24}(SH)_{18}^{q}$ (MAg_{24}), and $MAu_{37}(SH)_{24}^{q}$ (MAu_{37}) where M includes Ni, Pd and Pt (Group X), Cu, Ag and Au (Group XI), Zn, Cd and Hg (Group XII), and Ga, In and Tl (Group XIII) dopants. The possible dopant positions in the case of MAu_{24} or MAg_{24} are illustrated in Figure 1. In these systems, isomer I, isomer II and isomer III refer to the cases when the dopant occupies the central, core-surface or ligand-shell positions respectively, as shown in Figure 1. In the case of MAu_{37}, there are four symmetrically inequivalent isomer II and three symmetrically inequivalent isomer III positions, which are illustrated in Figure S1 of the Supplementary Information (SI). For MAu_{24} and MAg_{24} systems, the charges are selected in order to obtain the $1S^21P^61D^0$ electronic structure, which is isoelectronic to the Au_{25}^{-1} or Ag_{25}^{-1} parent system. As a result, total charges of the clusters (q) are -2, -1, 0 and +1 for Group X, Group XI, Group XII and Group XIII dopants, respectively. For MAu_{37}, charges are similarly selected so that the doped cluster is isoelectronic to the neutral Au_{38} cluster. All calculations are performed for the singlet configurations of these charge states. It should be noted that these charges can be different from experimentally obtained charges for the clusters as in the case of $PdAu_{24}$ and $PtAu_{24}$,[45] where the neutral system is preferred ($1S^21P^4$) instead of -2 charge state ($1S^21P^6$). Nevertheless, the total charges of the investigated clusters are assigned according to preferred electronic structure of parent clusters for consistency.

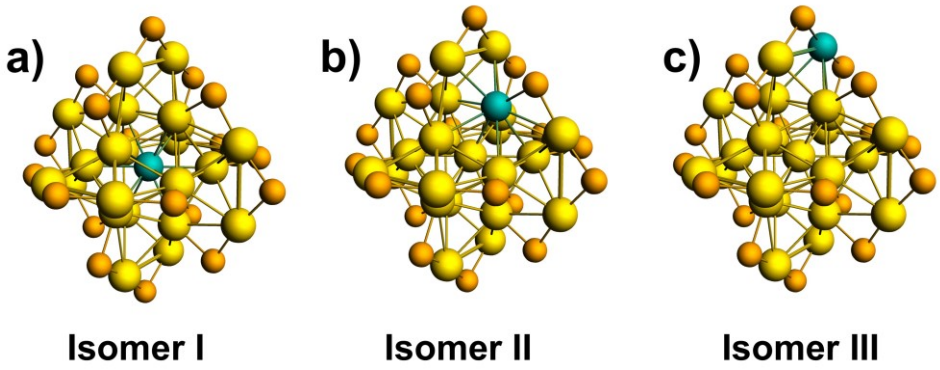

Figure 1. Illustration of isomer structures for doped MAu_{24} and MAg_{24} clusters using ball and sticks model. Ligands are removed from the pictures for clarity.

Calculations were performed using density functional theory (DFT) at the PBE/TZP level of theory.[59-60] The frozen core approximation was applied to the core electrons of the elements. For the geometry optimizations, the energy and gradient convergence thresholds were set to $1x10^{-}$

^{4} and $1x10^{-3}$ respectively. Additionally, the integral accuracy is increased to 7 within the Voronoi quadrature scheme. For the isomer I structure of MAu_{24} and MAg_{24}, C_i point-group symmetry was adapted in the starting geometries, whereas no symmetry constraint was employed for isomer II or III structures or in MAu_{37} structures. Relativistic effects were included using the zeroth-order regular approximation (ZORA) Hamiltonian at the scalar level.[61-63] The computations were carried out by using the Amsterdam Density Functional (ADF) 2016 or 2017 package.[64-66]

RESULTS AND DISCUSSION

1.1. Relative Isomer Energies and Geometries for MAu_{24}

In Table 1, we show the relative isomer energies and HOMO-LUMO gaps for the isomer I and isomer II species of different MAu_{24} systems. In the case of all group X dopants (M=Ni, Pd and Pt), isomer I is predicted to be more stable than isomer II. The energy difference between the two isomers is quite large for Ni and Pt doped clusters (19.3 and 26.4 kcal/mol for $NiAu_{24}^{-2}$ and $PtAu_{24}^{-2}$, respectively), whereas the same energy difference is somewhat smaller for the Pd doped cluster (8.7 kcal/mol). There is a correlation between the calculated HOMO-LUMO gaps of group X doped clusters and their relative isomer energies as well. For $NiAu_{24}^{-2}$ and $PtAu_{24}^{-2}$, calculated HOMO-LUMO gaps are 0.57 and 0.61 eV larger respectively for the isomer I structure compared to the HOMO-LUMO gaps that are calculated for the isomer II structure. In the case of $PdAu_{24}^{-2}$, this difference in HOMO-LUMO gaps of different isomers is smaller (at only 0.28 eV) compared to $NiAu_{24}^{-2}$ and $PtAu_{24}^{-2}$.

Table 1. Relative Isomer Energies and HOMO-LUMO Gaps for Doped MAu_{24}^{q} Systems, Relative Single-Point Isomer Energies of Doped Species in the Au_{25}^{-1} Geometry, and Reorganization Energies (ΔE_{reorg}) from the Au_{25}^{-1} Geometry to the Optimized MAu_{24}^{q} Geometry

MAu_{24}^{q} clusters	Isomer Energies (kcal/mol)		HOMO-LUMO Gap (eV)		Isomer Energies in Au_{25}^{-1} geometry (kcal/mol)		ΔE_{reorg} (kcal/mol)	
	Isomer I	Isomer II	Isomer I	Isomer II	Isomer I	Isomer II	Isomer I	Isomer II
Group X								
$NiAu_{24}^{-2}$	0.0	19.3	1.25	0.68	7.4	30.6	7.4	11.3
$PdAu_{24}^{-2}$	0.0	8.7	1.28	1.00	1.4	11.4	1.4	2.7
$PtAu_{24}^{-2}$	0.0	26.4	1.56	0.95	2.0	31.4	2.0	5.0
Group XI								
$CuAu_{24}^{-1}$	0.0	-4.2	1.09	1.31	3.9	-0.2	3.9	4.0
$AgAu_{24}^{-1}$	0.0	-16.2	1.06	1.27	0.0	-14.9	0.0	1.3
Group XII								
$ZnAu_{24}$	0.0	-8.7	1.03	1.30	2.5	-4.2	2.5	4.5
$CdAu_{24}$	0.0	-18.0	0.99	1.25	2.4	-15.3	2.4	2.7
$HgAu_{24}$	0.0	-14.0	1.14	1.13	1.8	-11.1	1.8	2.9
Group XIII								
$GaAu_{24}^{+1}$	0.0	-2.5	1.18	0.90	2.1	2.9	2.1	5.3
$InAu_{24}^{+1}$	0.0	-9.9	1.00	0.86	5.0	-2.1	5.0	7.9
$TlAu_{24}^{+1}$	0.0	-25.9	1.01	0.78	5.2	-9.4	5.2	16.6

Unlike group X dopants, for all group XI (M=Cu, Ag), group XII (Zn, Cd and Hg) and group XIII (M=Ga, In and Tl) dopants, isomer II is predicted to be more stable compared to the isomer I structure. In general, the energy differences between isomers are smaller for period 4 dopants (M=Cu, Zn and Ga), and vary between 2.5-8.7 kcal/mol. For heavier dopants, (M=Ag, Cd, Hg, In and Tl), the same energy differences become larger while varying between 9.9-25.9 kcal/mol. For group XI and XII dopants, calculated HOMO-LUMO gaps for the isomer II structure are larger than those calculated for the isomer I structure except for $HgAu_{24}$. In the case of $HgAu_{24}$, calculated HOMO-LUMO gaps are almost identical for isomer I and isomer II structures, while isomer II is predicted to be a significantly more stable structure. In the case of group XIII dopants, the calculated HOMO-LUMO gaps are smaller for the isomer II structure despite the fact that this structure is predicted to more stable compared to isomer I.

In Figure 2a and 2b, we show the correlation between the metallic radii of dopants[67] and the average M-Au bond lengths within the MAu_{12} core for the isomer I and isomer II structures of doped MAu_{24} clusters, respectively. In the case of the isomer I geometry, there is a very good linear correlation between the metallic radii of dopants and the M-Au bond lengths (R^2=0.95). The average M-Au bond lengths vary between 2.77-2.94 Å, indicating that the MAu_{12} core expands considerably as the metallic radius of the dopant becomes larger. The smallest and largest average bond lengths are predicted for Ni and Tl, which have the smallest (1.24 Å) and largest (1.70 Å) metallic radii respectively among the investigated dopants. For the isomer II geometry, the linear correlation becomes somewhat worse (R^2=0.85) compared to the correlation obtained for isomer I. In this case, the calculated average M-Au bond lengths vary between 2.78-3.37 Å, which shows a significant increase over the bond-length variation in the isomer I structure. The good correlation between metallic radii and M-Au bond lengths in both isomer structures may suggest that the bonding interaction has primarily metallic character within the core of MAu_{24} systems.

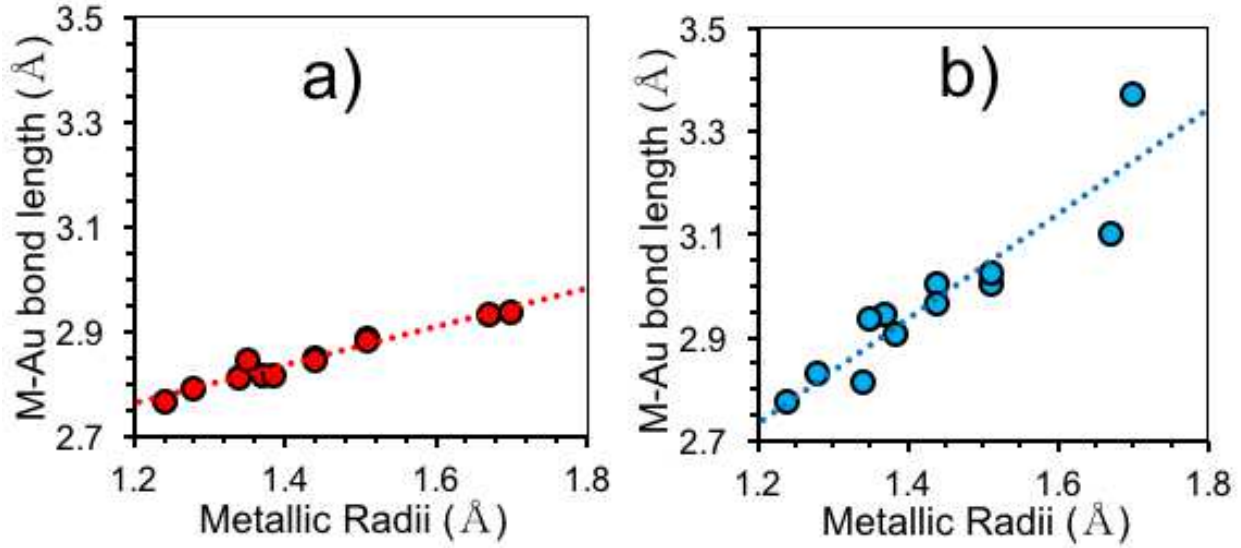

Figure 2. The correlation between metallic radii and M-Au bond lengths of the MAu_{12} core in doped MAu_{24} clusters for a) isomer I and b) isomer II structures. Dotted lines represent the best-fit correlation lines in both cases. The equations of the best-fit lines are y=0.37x+2.32 for isomer I and y=1.02x+1.51 for isomer II.

It is possible to decompose the energy difference between the isomers into two parts: an electronic contribution that results from changes in the electronic structure as a result of doping

without any relaxation in the geometry, and the reorganization energy (ΔE_{reorg}), which refers to the energy stabilization due to the relaxation of the geometric structure compared to the initial structure, where the initial structure refers to the MAu_{24}^{q} system in the **parent Au_{25}^{-1}** cluster geometry. In Table 1, we tabulate the relative isomer energies of doped systems in the Au_{25}^{-1} geometry and the ΔE_{reorg} energies of the two different isomers. For all cases except $GaAu_{24}^{+1}$, the ordering of the stabilities for isomer I and isomer II structures of doped systems with the Au_{25}^{-1} geometry does not change compared to the relative ordering of isomers in their fully relaxed geometries (Table 1). For $GaAu_{24}^{+1}$ in the Au_{25}^{-1} geometry, isomer I is predicted to be more stable, which was not the case as shown in Table 1 for fully relaxed geometries. However, we also note that the predicted energy difference between isomers for this system are quite small regardless of the geometry of the system and are within the usual uncertainty ranges of DFT.

For all doped systems, ΔE_{reorg} are larger for isomer II structures when compared to the ΔE_{reorg} that are obtained for isomer I structures. This is expected since the overall geometry of the cluster has more degrees of freedom in the isomer II structure as a result of lowering the symmetry compared to the isomer I structure. The effect of symmetry lowering is also seen for the variation in calculated M-Au bond lengths as shown in Figure 2. As a result, the relative isomer energies shift in favor of isomer II from their starting Au_{25}^{-1} geometry to their fully relaxed geometry. Moreover, we note a positive correlation between the ΔE_{reorg} and the metallic radii of the dopant. For example, ΔE_{reorg} are largest for Ni and Tl doped systems, where the metallic radii of the dopants exhibit the largest deviation from the metallic radius of Au. In comparison, ΔE_{reorg} are smallest for both isomers in the case of the Ag doped cluster, where the deviation between the dopant metallic radius and Au metallic radius is smallest. These results indicate that the metallic radii of the dopants can play an important role in determining the relative energies of the isomers, especially when the dopant metallic radius deviates significantly from the metallic radius of Au, such as the case for the $TlAu_{24}$ cluster. However, for most of the systems investigated, the relative stabilities of isomers are already determined by the changes initially introduced in the electronic structure by the dopant before the geometry is relaxed, as indicated by the results shown in Table 1.

1.2. Discussion of Electronic Structures for MAu_{24} systems

Group XI dopants: $AuAu_{24}^{-1}$, $AgAu_{24}^{-1}$ and $CuAu_{24}^{-1}$

In this section, we will investigate the effect of doping on the electronic structure of MAu_{24} for different dopants. As a starting point, we apply fragment calculations (see computational methods and SI for details) for the pseudo-doped $AuAu_{24}^{-1}$ clusters. These calculations provide a way to distinguish between the contributions of one particular atom (either an Au atom or a different metal dopant) and the remainder of the core for analyzing the electronic structure of the entire system. In the $AuAu_{24}^{-1}$ cluster, isomer I refers to the case when the Au atom occupying the center of the Au_{13} core is treated as the dopant, whereas isomer II refers to the case when an Au atom in a surface position is treated as the dopant. In Figure 3, we illustrate the relative weights of atomic orbitals from the dopant Au and of super-atomic S, P and D orbitals in the Au_{12} core for energy levels of the Au_{25}^{-1} cluster. For simplicity, contributions from the ligand shell and the Au d band are not shown individually in Figure 3.

As shown in Figure 3, the coupling between atomic orbitals of the dopant Au and the super-atomic orbitals shows significant variation between isomer I and isomer II. When the central Au atom is treated as the dopant (isomer I), the atomic s orbital of Au contributes significantly to the 1S level. Similarly, atomic p and atomic d levels couple with P and D super-atomic orbitals of the Au_{12} core to yield the 1P and 1D levels of the cluster, respectively. In comparison, the s orbital

contribution is largely reduced when one of the Au atoms on the core-surface is treated as the dopant in the fragment calculation (isomer II). In this case, atomic s and d orbitals exhibit coupling with the super-atomic P orbitals. For the 1D level, the interaction is mainly between Au s orbitals and super-atomic D orbitals, with a small contribution from Au p orbitals. The different interaction picture for the two-fragment scheme is, of course, a result of symmetry considerations. When the dopant Au is in the center, the angular momentum of the atomic levels of the Au atom and the super-atomic levels of Au_{12} should match for a non-zero overlap between these levels. These symmetry restrictions are lifted in the case of isomer II, which affects the interaction picture between atomic and super-atomic levels.

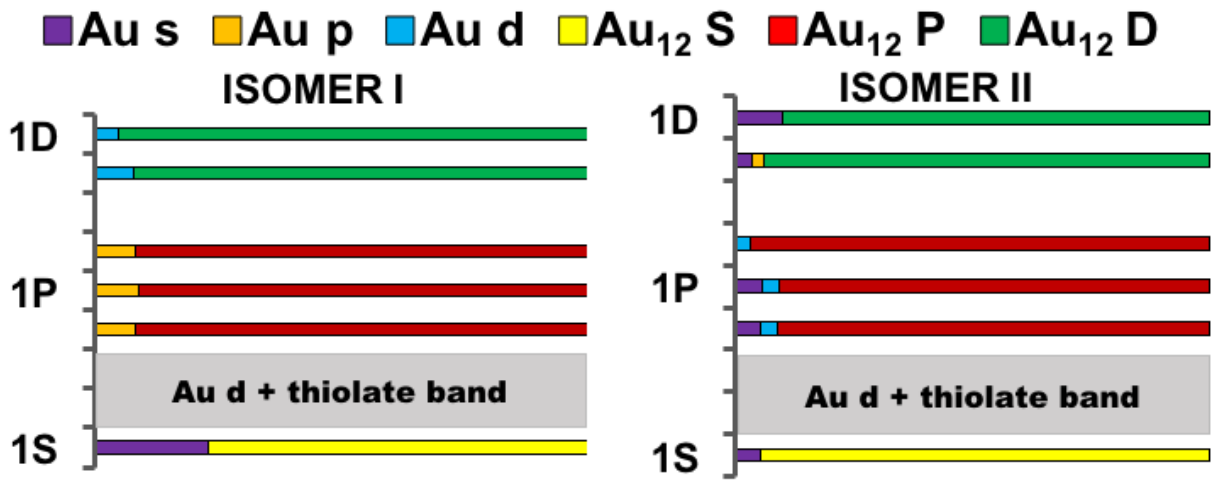

Figure 3. Comparison of the relative weights of s, p and d atomic orbitals from the dopant (Au) and from the S, P and D super-atomic orbitals originating from the remaining Au_{12} core in the electronic structures of isomer I and isomer II of $AuAu_{24}^{-1}$.

For the other group XI dopants (Ag and Cu), isomer II is predicted to be more stable compared to isomer I as shown in Table 1. The geometric effects are quite small for these dopants as indicated by the calculated ΔE_{reorg} (Table I). This result indicates that the major contribution for the isomer stabilities arises from electronic effects rather than geometric effects. In Figure 4, we show the comparison of electronic structures for isomer I and isomer II of the MAu_{24}^{-1} system where M=Cu or Ag. There is a good correlation between the relative stability of isomers and the energies of the super-atomic levels of the cluster; from isomer I to isomer II the occupied 1P and 1S levels become energetically more stable (leading to an increase in stability of the system), whereas the unoccupied 1D levels become less stable. The total stabilization of the 1P levels is calculated to be 0.40 eV, whereas the 1S level becomes more stable by 0.51 eV when the electronic structures of isomer I and isomer II are compared for the $AgAu_{24}^{-1}$ cluster. In comparison, the stabilization of the 1P and 1S levels are 0.22 eV and 0.24 eV respectively for $CuAu_{24}^{-1}$.

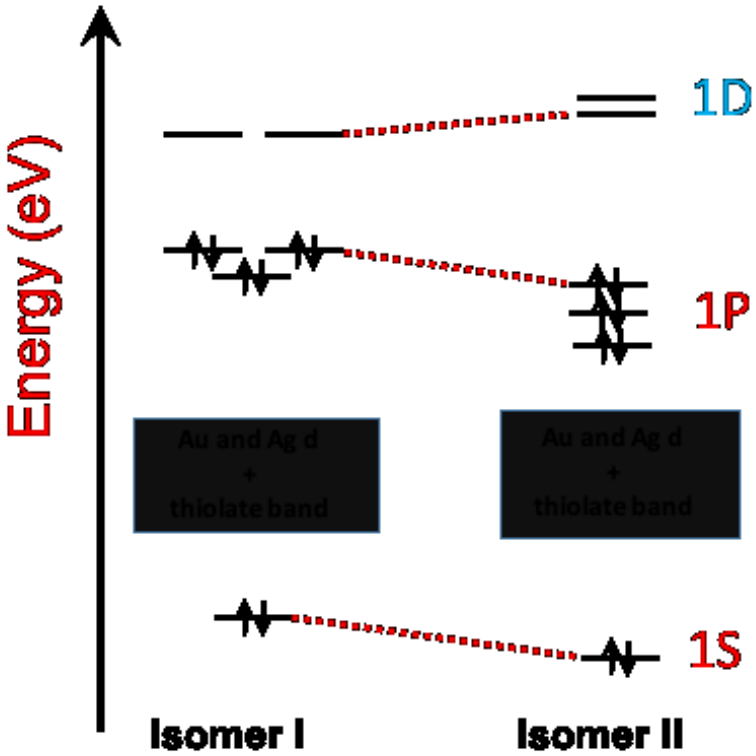

Figure 4. Illustration of the energy change for the 1S, 1P and 1D levels with varying dopant position in the case of Group XI dopants.

For a more detailed understanding of electronic effects introduced by dopants, we show the coupling between Ag/Cu atomic orbitals (dopant) and Au_{12} super-atomic orbitals for isomer II and isomer I structures of doped MAu_{24}^{-1} in Figure 5. Contributions from fragments are tabulated in Table S1 of the SI. For isomer I, atomic Ag/Cu s, p and d orbitals only couple with super-atomic S, P and D levels respectively as shown in Figure 5 because the dopant sits in the center of the cluster. Therefore, only s-S, p-P or d-D coupling is allowed between the dopant and the Au_{12} core levels due to symmetry. In comparison, dopant and super-atomic levels that have different angular momentum can couple in the isomer II structure. In this case, Ag s and d orbitals couple with the super-atomic P levels for the 1P level of the cluster instead of the Ag p orbitals. Additionally, the contribution of Ag s orbitals to the 1S level is significantly reduced in the isomer II geometry compared to the case in isomer I. This is generally the case for $CuAu_{24}^{-1}$ as well. One main difference is that the Cu d contribution to 1P levels is considerably larger in isomer II of $CuAu_{24}^{-1}$ compared to the Ag d contribution to 1P levels for the same isomer in $AgAu_{24}^{-1}$. This is most likely due to the fact that Cu d levels are higher in energy compared to the Ag d levels, which results in more efficient coupling for the low-lying states for the former case.

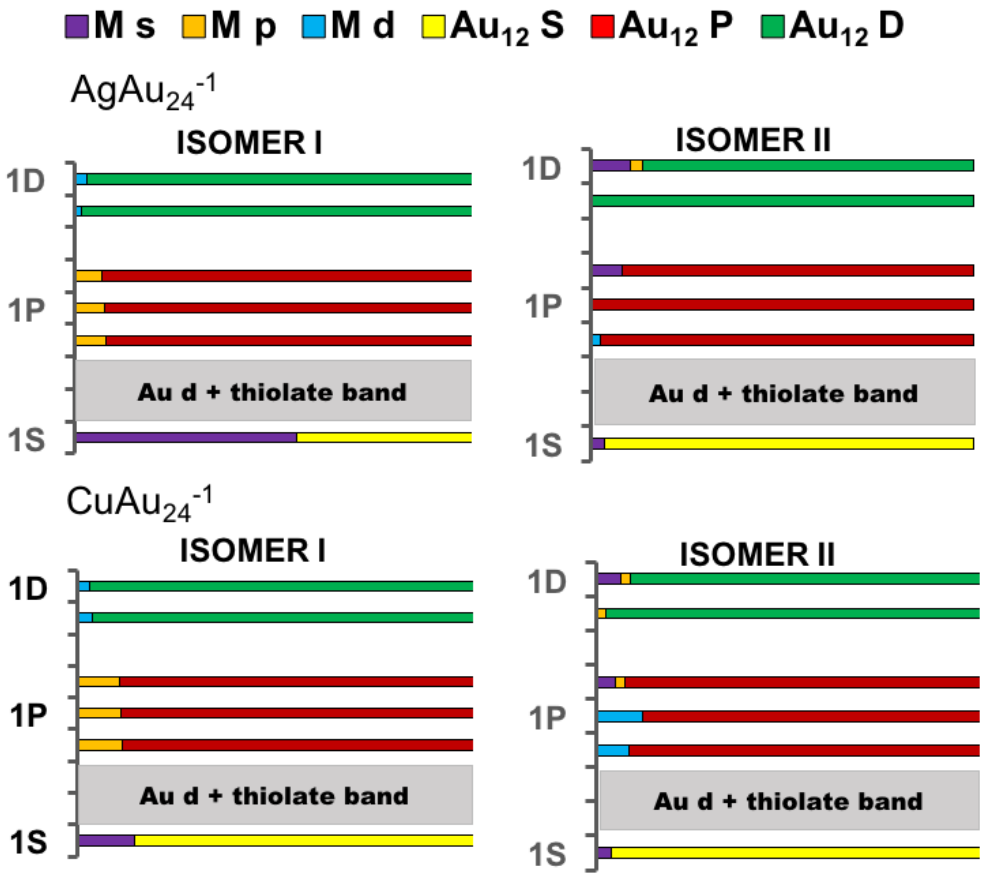

Figure 5. The comparison for the relative weights of s, p and d atomic orbitals from dopant (Ag and Cu) and S, P and D super-atomic orbitals originating from Au_{12} core in the case of isomer I and isomer II electronic structures of $AgAu_{24}^{-1}$ and $CuAu_{24}^{-1}$.

The difference in the contribution of dopant atomic orbitals when occupying different positions in the cluster can also be seen in the calculated partial Mulliken populations shown in Table 2. In the table, ΔQ refers to the Mulliken population difference on the dopant between the isomer I (Q_I) and isomer II (Q_{II}) structures ($\Delta Q = Q_{II} - Q_I$). As the dopant switches position from center (isomer I) to core-surface (isomer II), there is a decrease in the partial Mulliken populations for orbitals with s and p angular momenta. This is a result of the smaller coupling between atomic Au s and p orbitals with super-atomic S and P levels in the case of isomer II compared to isomer I. In comparison, the d population on dopants becomes larger from isomer I to isomer II as some dopant d contribution transfers from unoccupied 1D levels to occupied 1P levels in isomer II. For all systems, the total Mulliken charge becomes smaller for the dopant in isomer II, when compared to the case in isomer I. These results show that the relative dopant character in the super-atomic levels of the cluster depends strongly on the isomer type.

Our analysis for the electronic structure of Cu and Ag doped Au_{25}^{-1} clusters indicate that the relative stabilities of the isomers and their energy levels can be linked to the changes in the coupling between super-atomic S and P orbitals that originate from the Au_{12} core and the atomic s, p and d orbitals of the dopant in different isomers. As shown in Figures 4 and 5, the contribution of atomic s and p orbitals from the dopant in isomer I is largely replaced by the contributions from the central Au in isomer II. At this point, the trends in the energetics of 1S and 1P levels and the overall isomer energies can be understood from the trends in periodic table and relativistic effects.

From Cu to Ag, the valence d orbitals become more stable due to the larger nuclear charge, whereas valence s and p levels become less stable due to the more effective shielding of d orbitals in Ag. In comparison, valence s and p levels are largely stabilized in Au compared to Ag and Cu due to scalar relativistic effects, which is known as the s and p contraction.[68] These effects for the atomic levels are shown for Cu, Ag and Au in Figure S3. As a result, the 1S and 1P levels of the clusters undergo a larger relativistic stabilization in isomer II due to the larger Au s and p contribution, compared to the case in isomer I.

Table 2. Partial Mulliken Populations and Total Mulliken Charges on the Group XI Dopants for Different Isomer Structures of MAu_{24} Systems.

Dopant Atom	Total Charge	Partial Populations		
		s	p	d
		Cu		
Isomer I	-0.66	0.91	1.10	9.66
Isomer II	0.05	0.48	0.65	9.82
ΔQ	0.71	-0.43	-0.44	0.17
		Ag		
Isomer I	-0.67	1.42	0.66	9.59
Isomer II	-0.07	0.81	0.46	9.80
	0.60	-0.61	-0.20	0.20
		Au		
Isomer I	-0.52	3.09	6.92	9.51
Isomer II	0.14	2.74	6.49	9.63
ΔQ	0.66	-0.35	-0.43	0.12

These results can be further supported by the comparison of energy levels and the relative isomer stabilities predicted by non-relativistic DFT and scalar-relativistic DFT. As shown in Table 1, isomer II of $AgAu_{24}^{-1}$ clusters is predicted to be more stable by 14.9 kcal/mol when the ZORA scalar relativistic Hamiltonian is employed. In comparison, the same isomer is predicted to be more stable by only 2.3 kcal/mol with non-relativistic DFT. Similar to the case in $AgAu_{24}^{-1}$, the energy difference between isomer I and isomer II reduces from 4.1 kcal/mol to 0.4 kcal/mol for $CuAu_{24}^{-1}$ when a non-relativistic Hamiltonian is employed instead of the ZORA scalar relativistic Hamiltonian. These results clearly show that the relative isomer energies of these systems are mainly determined by the combination of symmetry considerations and relativistic effects on the electronic structure of MAu_{24}^{-1} clusters.

Group X dopants: $NiAu_{24}^{-2}$, $PdAu_{24}^{-2}$ and $PtAu_{24}^{-2}$

In the case of group X dopants, isomer I is predicted to be the most stable isomer unlike the case in other dopants investigated in this work. The main difference in the electronic structure of Ni, Pd and Pt doped MAu_{24} clusters and the electronic structure of group XI, XII and XIII doped MAu_{24} clusters is the presence of nd levels, which originate mainly from the atomic d orbitals of the dopant, as illustrated in Figure 6 for $PtAu_{24}^{-2}$. For isomer I, the nd levels show mixing with super-atomic D levels as a result of symmetry considerations, whereas they can mix with P levels in isomer II (Figure 6b). We also note this alteration in the interaction picture leads to an overall destabilization of the frontier levels in isomer II, compared to the case in isomer I. Similar results have been found for other group X dopants and previously investigated group IX (Co, Rh and Ir)

dopants, where the interaction of nd levels with super-atomic levels mainly determine the stability of isomers for doped clusters.[58] Additionally, the energy separation between isomers can be linked to the energies of the d-shell for the dopants. As shown in Table 1, the energy difference between isomer I and isomer II is significantly higher for Ni and Pt doped clusters compared to the case for Pd.

It should also be noted that the experimentally obtained $PtAu_{24}$ and $PdAu_{24}$ clusters are suggested to exhibit neutral charges[44, 45] instead of the -2 charge used in this work. While the charge state can alter the calculated energy differences between two isomers, isomer I is still expected to be the more stable isomer for these systems since the symmetry-dictated mixing between nd levels and super-atomic levels will be quite similar in the neutral charge state as well. In fact, calculated energy differences for the neutral charge states of the isomers of $PtAu_{24}$ and $PdAu_{24}$ clusters also show that the isomer I structure is favored by 13.1 and 6.2 kcal/mol respectively. Similar results for the different charge states of group IX (Co, Rh and Ir) doped clusters have been shown as well.[58]

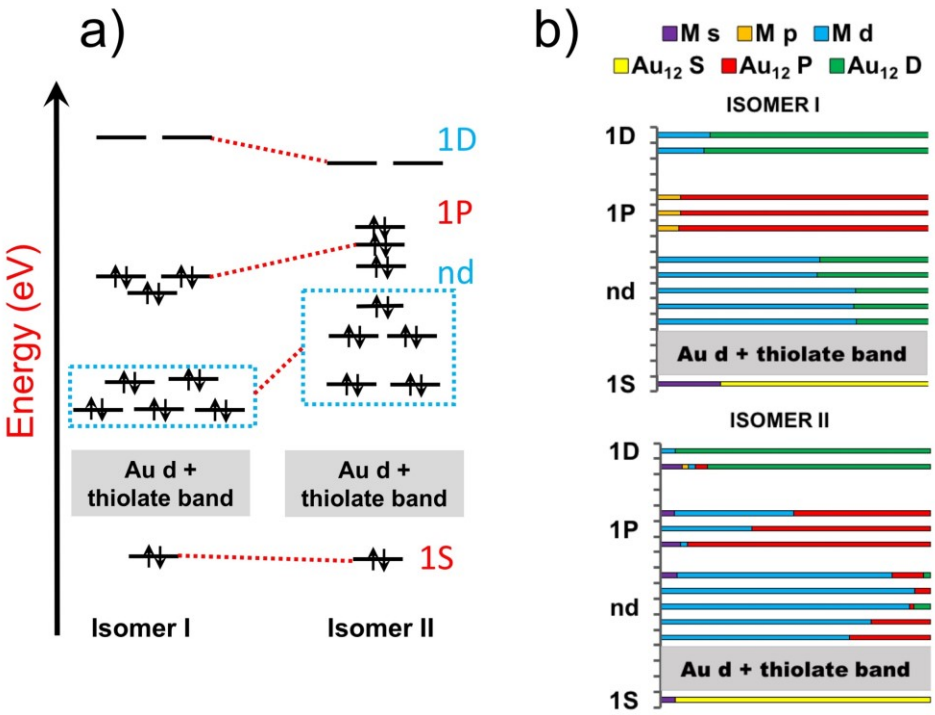

Figure 6. a) Illustration of the energy change for the 1S, 1P and 1D and nd levels with varying dopant position in the case of Group X dopants and b) comparison of the relative weights of s, p and d atomic orbitals from Pt as well as S, P and D super-atomic orbitals originating from the Au_{12} core for the isomer I and isomer II electronic structures of $PtAu_{24}^{-2}$.

Group XII dopants: $ZnAu_{24}$, $CdAu_{24}$ and $HgAu_{24}$

Similar to the group XI dopants (Ag and Cu), isomer II is predicted to be more stable compared to isomer I for all group XII dopants (Zn, Cd and Hg). In Figure 7, we illustrate the interaction picture between the dopant atomic orbitals and the super-atomic levels originating from the Au_{12} core for the $CdAu_{24}$ doped cluster. In all cases, the dopant s and p orbitals couple with

super-atomic S and P levels respectively for the isomer I structure, similar to the case in the Ag and Cu doped clusters. In comparison, dopant d orbitals for Zn, Cd and Hg do not contribute to 1D levels as the atomic d orbitals of the group XII elements are energetically more stable compared to the group XI and X elements. For isomer II, s-S and p-P coupling between dopant orbitals and Au_{12} super-atomic levels decrease significantly due to symmetry lifting, similar to the case in group XI dopants. On the other hand, the contribution of dopant s orbitals to unoccupied 1D levels shows an increase for group XII dopants when compared to group XI dopants. In Table S2, we show the calculated partial Mulliken populations and total Mulliken charges for group XII dopants. Similar to the case in group XI dopants (Table 2), s and p populations decrease whereas d populations show a slight increase for all group XII dopants when changing from isomer I to isomer II structures.

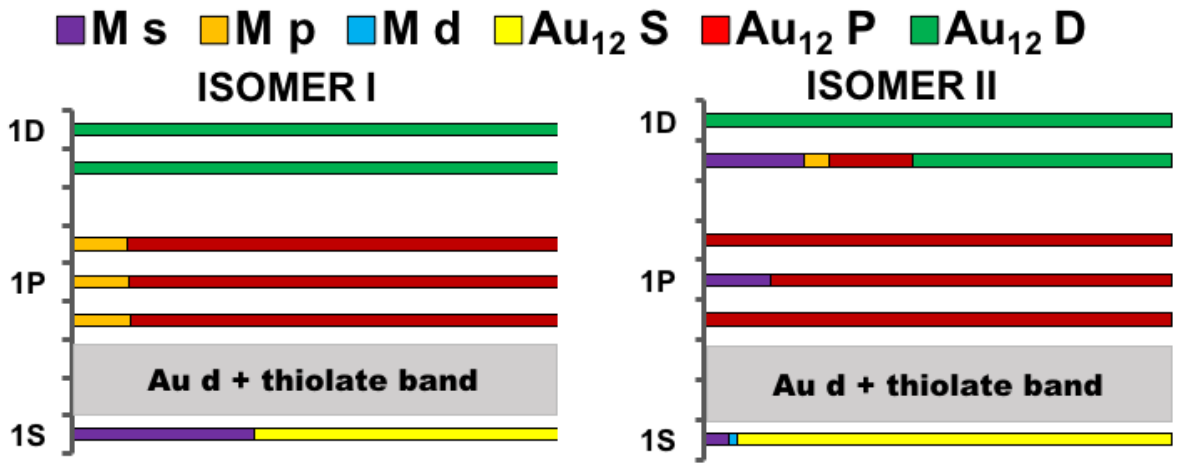

Figure 7. Comparison of the relative weights of s, p and d atomic orbitals from Cd and S, P and D super-atomic orbitals originating from the Au_{12} core in electronic structures of isomer I and isomer II of $CdAu_{24}^{0}$.

Comparison of the electronic structures for the isomer I and isomer II structures of the MAu_{24} clusters (M=Zn, Cd, Hg) reveals that 1P energy levels become more stable in isomer II. This is again related to the fact that 1P levels have more Au p character respectively in isomer II when compared to isomer I as shown in Figure 7 for the Cd of group XII dopants. The total stabilization of 1P levels from isomer I to isomer II is 0.27, 0.30 and 0.16 eV for Zn, Cd and Hg respectively. The 1S level also becomes more stable for isomer II for Zn and Cd doped clusters by 0.16 and 0.12 eV respectively. However, it becomes somewhat less stable for the Hg doped cluster by 0.11 eV. This is most likely due to the relativistic contraction of the Hg s orbitals, which stabilize the 1S level in the isomer I structure of the $HgAu_{24}$ cluster. On the other hand, the relativistic contraction of the valence p orbitals of Hg is less obvious compared to the case in Au,[68] which results in less stable 1P levels for the isomer I structure of the $HgAu_{24}$ cluster. Nevertheless, our results for group XII dopants show that the stability of isomer II over isomer I is mainly determined by group theory and relativistic effects as well.

Group XIII dopants: Ga, In and Tl

The contribution of dopant orbitals exhibits significant changes for group XIII dopants compared to other investigated systems, especially in the case of the isomer II structure of the doped clusters. In Figure 8, we illustrate the interaction picture between the dopant atomic orbitals, and super-atomic levels originating from the Au_{12} core for the 1S, 1P and 1D levels of $InAu_{24}^{+1}$.

We again note that a similar interaction picture is obtained for Ga and Tl doped systems. For isomer I, s-S and p-P coupling is observed for the 1S and 1P levels, whereas no d-D coupling is observed for the 1D levels since dopant d orbitals for group XIII elements are mainly core levels and do not contribute to bonding interactions. It is also seen that the dopant s and p orbital contribution is increased for group XIII dopants when compared to the same contributions for group XI and group XII dopants in isomer I. For isomer II, the dopant s orbital contributes significantly to 1P levels and 1D levels as shown in Figure 9a and 9b respectively. Similar to the previously investigated cases, these results are also evident from the calculated partial Mulliken populations given in Table S2. In general, the total Mulliken charge on the dopant significantly decreases from isomer I to isomer II, which is largely the result of lost p electron population in the 1P levels of the cluster.

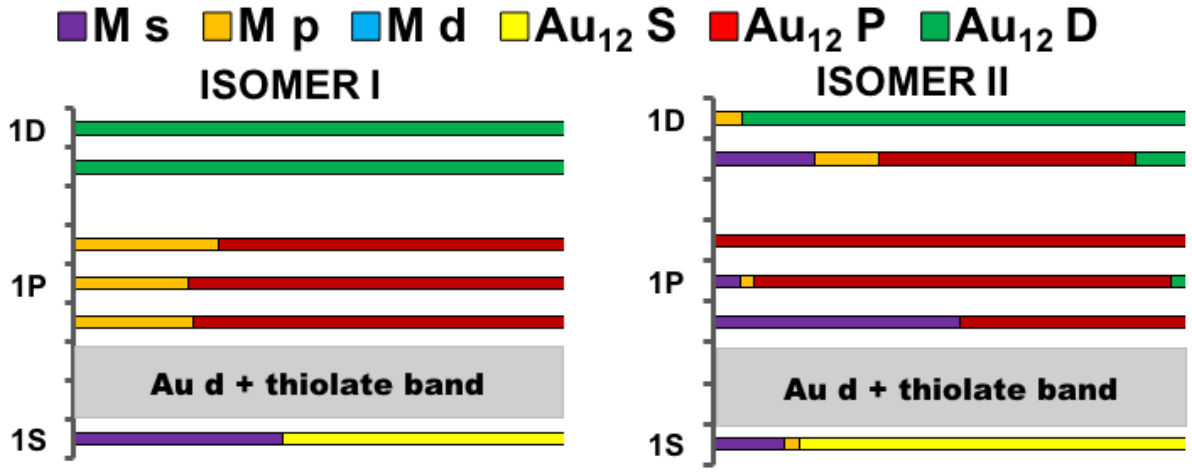

Figure 8. Comparison of the relative weights of s, p and d atomic orbitals from In and S, P and D super-atomic orbitals originating from the Au_{12} core in the electronic structures of isomer I and isomer II of $InAu_{24}^{+1}$.

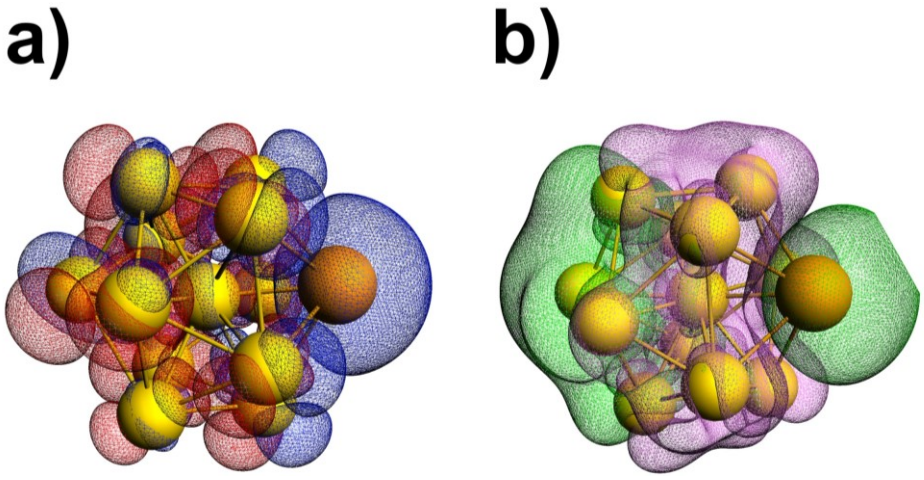

Figure 9. Illustration of coupling between In s orbital and super-atomic P orbital in $InAu_{24}^{+1}$ cluster for a) 1P level which can be regarded as a bonding combination of s and P, and b) 1D level which can be regarded as an antibonding combination of s and P. We also note that the 1P and 1D level that have the largest dopant

s contributions are significantly more stable compared to other 1P and 1D levels (not shown here) respectively. The ligand-shell contributions to MOs are not displayed for the clarity of the image.

1.3. Comparison of doped Ag_{25} and Au_{25} clusters

In the previous section, we have shown that relativistic effects and group theory play important roles in the doping process of Au_{25} clusters. Since Ag is often regarded as non-relativistic Au,[68-69] one would expect significant changes in the relative stability of isomers between doped MAg_{24} and MAu_{24} clusters. In Figure 10, this difference is illustrated for the two clusters by showing the comparison between relative isomer energies (ΔE_{isomer} = E[isomer II]-E[isomer I]) for the two clusters. We also tabulate the relative isomer energies, HOMO-LUMO gaps and ΔE_{reorg} in Table 3 for the investigated MAg_{24} clusters.

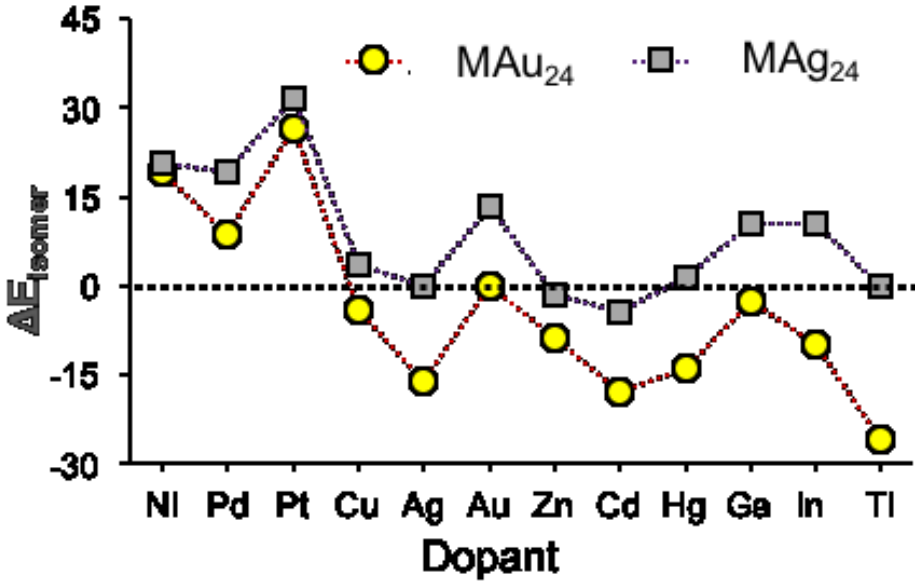

Figure 10. Comparison of ΔE_{isomer} (E[isomer II]-E[isomer I]) for MAu_{24} and MAg_{24} doped clusters.

In general, there is a very good correlation between ΔE_{isomer} values of doped MAg_{24} and MAu_{24} clusters for the different dopants across the periodic table. However, the key difference between MAg_{24} and MAu_{24} is that ΔE_{isomer} of MAg_{24} is shifted in favor of the isomer I structure to more positive energies compared to the case in MAu_{24}. This is related to the fact that the energy penalty for exchanging the central Ag atom with the dopant is not as large compared to the exchange of the central Au atom with the dopant, as previously described for MAu_{24}, which is dictated by the presence or lack of relativistic effects.

Table 3. Relative Isomer Energies and HOMO-LUMO Gaps for Doped MAg_{24}^{q} Systems, Relative Single-Point Isomer Energies of Doped Species in the Ag_{25}^{-1} Geometry, and the Reorganization Energies (ΔE_{reorg}) from the Ag_{25}^{-1} Geometry to the Optimized MAg_{24}^{q} Geometry

MAg_{24}^{q} clusters	Isomer Energies (kcal/mol)	HOMO-LUMO Gap (eV)	Isomer Energies in Ag_{25}^{-1} geometry (kcal/mol)	ΔE_{reorg} (kcal/mol)

	Isomer I	Isomer II	Isomer I	Isomer II	Isomer I	Isomer II	Isomer I	Isomer II
Group X								
$NiAg_{24}^{-2}$	0.0	20.6	1.45	0.73	6.3	36.6	6.3	16.0
$PdAg_{24}^{-2}$	0.0	19.2	1.45	1.08	2.3	24.1	2.3	5.0
$PtAg_{24}^{-2}$	0.0	31.7	1.65	1.01	2.4	41.3	2.4	9.6
Group XI								
$CuAg_{24}^{-1}$	0.0	3.6	1.41	1.40	3.1	9.8	3.1	6.2
$AuAg_{24}^{-1}$	0.0	13.4	1.58	1.33	0.2	14.5	0.2	1.1
Group XII								
$ZnAg_{24}$	0.0	-1.4	1.51	1.42	2.7	5.0	2.7	6.4
$CdAg_{24}$	0.0	-4.4	1.50	1.30	1.7	-2.4	1.7	2.0
$HgAg_{24}$	0.0	1.3	1.64	1.22	1.7	4.0	1.7	2.6
Group XIII								
$GaAg_{24}^{+1}$	0.0	10.6	1.76	1.17	5.4	20.3	5.4	9.6
$InAg_{24}^{+1}$	0.0	10.6	1.73	0.98	6.1	17.6	6.1	7.0
$TlAg_{24}^{+1}$	0.0	17.6	1.74	0.80	6.6	11.3	6.6	11.2

For a more detailed comparison of doping effects in MAg_{24} and MAu_{24}, we illustrate the changes in the electronic structure of isomer I and isomer II structures for $AuAg_{24}^{-1}$ in Figure 11, similar to the case in $AgAu_{24}^{-1}$ as shown in the previous section. Unlike the case in $AgAu_{24}^{-1}$ (Figure 4), the 1S and 1P energy levels for $AuAg_{24}^{-1}$ become more stable whereas 1D levels become less stable for isomer I compared to the energy levels of isomer II as shown in Figure 11a. As expected from the orbital energy levels, the isomer I structure is predicted to be more stable for this system by ~13 kcal/mol compared to its isomer II structure. Similar to the MAu_{24} cases, Figure 11b shows the coupling between Au (dopant) atomic orbitals and Ag_{12} super-atomic S, P and D orbitals for isomer I and isomer II structures of doped $AuAg_{24}^{-1}$. Again, the isomer I symmetry only allows s-S, p-P or d-D coupling for this case, whereas dopant and super-atomic levels with different angular momentum show coupling interactions in the isomer II structure. As a result, the contribution of Au atomic p orbitals to 1P levels of isomer I is replaced by contributions from d and s orbitals in the case of isomer II. For the 1S level, only the Au s orbital is involved in the case of isomer I, whereas both s and d orbitals contribute significantly to this level in the isomer II electronic structure. We note that the total weights of the Au s contribution are 0.15 and 0.07 in isomer I and isomer II respectively. However, the relative weight of the Au s contribution with respect to the Ag_{12} super-atomic S level is quite similar in both isomers as shown in Figure 11b.

These changes in the interaction picture are also evident from Mulliken populations, which are tabulated for all investigated MAg_{24} systems in Table S3 of the SI. In the case of $AuAg_{24}^{-1}$, partial p population on Au (dopant) decreases from isomer I to isomer II whereas partial d population increases in the same order. However, unlike the case for Ag in $AgAu_{24}^{-1}$, partial s population also shows an increase from isomer I to isomer II. This is most likely due to the large contribution of Au s orbitals to 1P levels in the isomer II structure. Additionally, Au s contribution to the 1S level does not show a significant decrease in $AuAg_{24}^{-1}$ compared to the case for Ag in $AuAg_{24}^{-1}$.

For group X dopants (Ni, Pd and Pt) in MAg_{24} systems, the isomer I structure is predicted to be the most stable isomer. Similar to MAu_{24}, the electronic structure of these systems shows nd

levels that lie close to the HOMO-LUMO gap and originate mainly from d orbitals of dopants. The nd levels also become less stable in the isomer II structure when compared to isomer I, similar to the previously discussed MAu_{24} systems.[58] One difference between MAg_{24} and MAu_{24} systems for group X dopants is that the energy difference between the two isomers are further shifted in favor of the isomer I structure by ~2-10 kcal/mol in MAg_{24} compared to MAu_{24}. This result is most likely related to the energy penalty (or gain) by replacing the central Au (or Ag) atom in their respective isomer I structures.

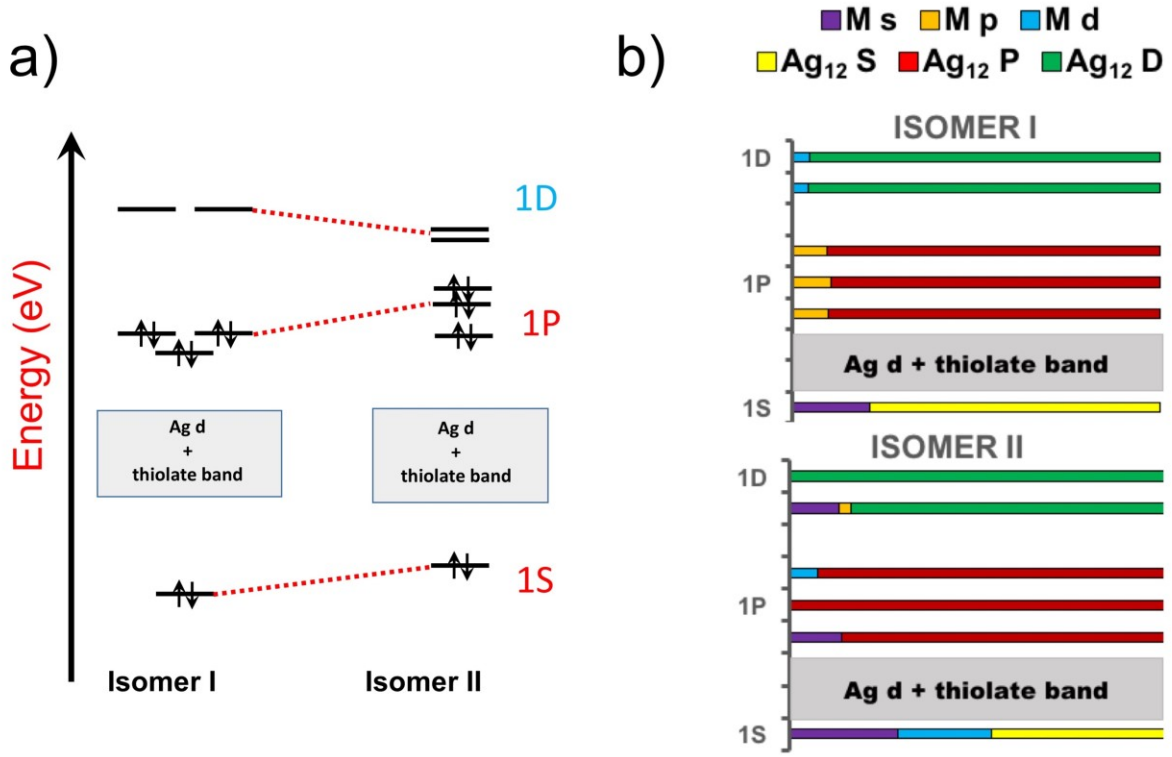

Figure 11. a) Illustration of the energy change for the 1S, 1P and 1D levels with dopant position for $AuAg_{24}^{-1}$ and b) comparison of the relative weights of s, p and d atomic orbitals from Au and S, P and D super-atomic orbitals originating from the Ag_{12} core in the case of isomer I and isomer II for $AuAg_{24}^{-1}$.

In the case of group XII (Zn, Cd and Hg) and group XIII (Ga, In and Tl) doped MAg_{24} systems, energy differences between the two isomers shift by ~7-25 kcal/mol in favor of isomer I compared to the isomer energy differences in MAu_{24} systems. As a result, the isomer I structure is predicted to be significantly more stable compared to isomer II for Ga and In doped MAg_{24}, whereas the isomer II structure has been shown to be more stable for MAu_{24} previously. For Zn, Hg and Tl doped MAg_{24} systems, DFT calculations show similar energies for isomer I and isomer II, where the energy difference between isomers are less than 1.5 kcal/mol for all cases. In comparison, isomer II is favored for $CdAg_{24}$ by ~4.5 kcal/mol. In general, our results show that the relative stabilities of isomers for the single metal doping of Ag_{25} and Au_{25} clusters show significant differences, which are mainly dictated by relativistic effects and orbital couplings arising from symmetry considerations for the dopant positions.

The metallic radii also affect the geometry of the MAg_{24} cluster significantly. This is illustrated in Figure S4 of the SI for MAg_{24} clusters. In general, there is a good linear correlation obtained between the metallic radii of dopants and the average M-Ag bond for both isomers with

a R^2 value of ~0.90. The slope of the correlation line shows a significant increase from isomer I to isomer II as in the case for the MAu_{24} cluster. This result can also be linked to the larger ΔE_{reorg} calculated for isomer II compared to those obtained for isomer I. Overall, the structural effects introduced by different dopants show good agreement between MAu_{24} and MAg_{24} clusters, which also emphasizes that the differences in relative isomer energies for MAu_{24} and MAg_{24} clusters are instead related to the differences in electronic and relativistic effects in Ag and Au atoms.

1.4. Comparison of doped Au_{25} and Au_{38} clusters

In Figure 12, we show the comparison of relative isomer energies (ΔE_{isomer}) for singly-doped MAu_{24} and MAu_{37} clusters. In the case of isomer II of MAu_{37}, we consider four different positions for the dopant (Figure S1), which are symmetrically inequivalent in the parent Au_{38} cluster geometry. The calculated energies for different isomer II geometries can vary by as much as 6 kcal/mol for MAu_{37} systems. In most cases, the absolute values of ΔE_{isomer} calculated for MAu_{37} are slightly smaller compared to those calculated for MAu_{24} systems, which may be linked to the symmetry considerations between singly-doped MAu_{37} and MAu_{24}. Nevertheless, Figure 12 shows that there is a very good agreement between ΔE_{isomer} of MAu_{24} and MAu_{37} clusters.

For a further analysis of relative isomer energies, we illustrate the electronic structure of the $AgAu_{37}$ system for isomer I and the most stable isomer II (isomer IId) in Figure 13a. As shown previously, the electronic structure of the Au_{38} cluster can be modelled as a super-atomic molecule arising from two super-atoms.[33] We have used the same model for the electronic levels of $AgAu_{37}$ in Figure 13. From isomer I to isomer II, Σ levels that originate from combinations of super-atomic S orbitals and Σ and Π levels that originate from combinations of super-atomic P orbitals become more stable similar to the case for 1S and 1P levels in $AgAu_{24}^{-1}$. In comparison, Δ levels become less stable in the isomer II electronic structure compared to the isomer I structure as in the case of the 1D level in $AgAu_{24}^{-1}$. The interaction picture shown in Figure 13b also illustrates the similarities between $AgAu_{24}^{-1}$ and $AgAu_{37}$ for the effect of doping in the electronic structure. Similar to the case in $AgAu_{24}^{-1}$, the s and p contributions of Ag to Σ and Π levels are reduced significantly from isomer I to isomer II, which results in the stabilization of these levels. Furthermore, we tabulate partial Mulliken charges for the doped MAu_{37} systems in Table S4. In the case of $AgAu_{37}$, partial s and p populations on Ag decrease by 0.53 and 0.12 respectively, whereas the d population increases by 0.18 from isomer I to isomer II, which shows a very good agreement with the changes in calculated partial populations on Ag in $AgAu_{24}^{-1}$ (Table 2).

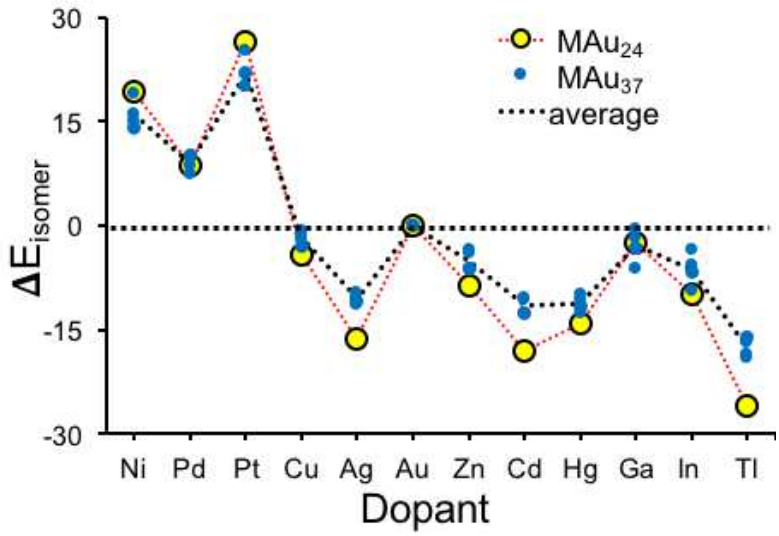

Figure 12. Comparison of ΔE_{isomer} for doped MAu_{24} and MAu_{37} clusters. In the case of MAu_{37}, blue circles represent the ΔE_{isomer} for different individual isomer II structures shown in the SI, whereas the blue dotted line passes through the average ΔE_{isomer} for this system.

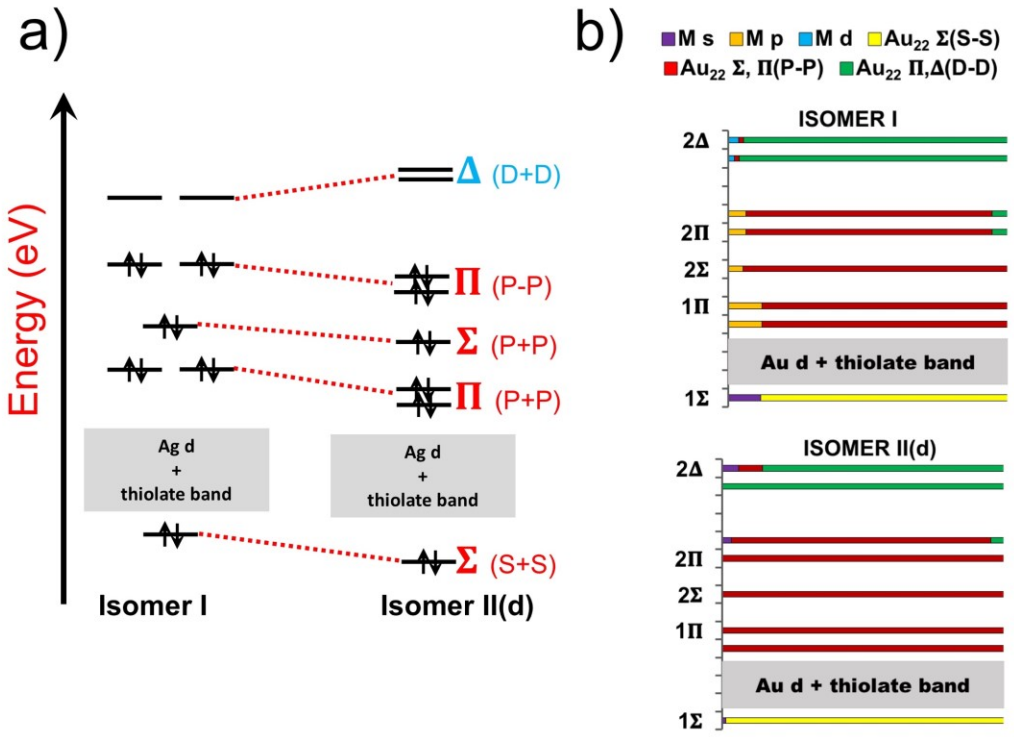

Figure 13. a) Illustration of the energy change for the Σ, Π, and Δ super-atomic molecular levels with dopant position in the case of the $AgAu_{37}^{0}$ cluster and b) the comparison for the relative weights of s, p and d atomic orbitals from Ag and super-atomic molecular levels originating from the remaining Au_{22} core in the case of isomer I and isomer II(d) for the same system.

The similarities for the doping process of MAu_{24} and MAu_{37} clusters are not limited to the case where M=Ag. In general, both the interaction picture and the calculated partial Mulliken charges are quite similar for the investigated MAu_{24} and MAu_{37} systems. For example, in the case of group X dopants, nd levels that originate from dopant d orbitals are significantly involved in the interaction picture of valence energy levels. Similar to the case in MAu_{24} or MAg_{24}, these interactions favor the isomer I structure for MAu_{37} as shown in Figure 12 as the nd levels become more stable when the dopant occupies the central position. For other dopants, the nd levels do not interact significantly with Σ and Π levels originating from the remaining Au_{22} core. In these cases, previously discussed symmetry effects and relativistic effects dominate isomer stability, similar to the case illustrated in Figure 11. As a result, the isomer II structure is mainly predicted to be more stable compared to isomer I for group XI-XIII dopants as shown in Figure 12.

1.5. Isomer III structure

While our previous discussion is limited to the comparison of isomer I and isomer II structures of doped MAu_{24}, MAg_{24} and MAu_{37} clusters, a dopant atom can also replace one of the Au or Ag atoms in the ligand shell (isomer III) as shown in Figure 1. In Table S5, we tabulate relative isomer energies of isomer III structures and HOMO-LUMO gaps for MAu_{24} and MAg_{24} systems. For group X dopants, low-lying nd levels again become significantly less stable in the isomer III structure compared to the case in isomer I for MAu_{24}, MAu_{37}, and MAg_{24}. A similar case has been illustrated for the nd levels of Co, Rh and Ir doped MAu_{24} clusters previously.[58] As a result, calculated relative energies of isomer III are quite similar to those calculated for isomer II for group X dopants, and isomer I structures are predicted to be the most stable isomer for these cases.

For other dopants, where nd levels do not interact with super-atomic levels, other factors such as the strength of RS-M-SR bonds in the ligand shell, or the energetics of 1S and 1P levels may be important for understanding the relative stabilities of isomer III. For example in the case of $AgAu_{24}^{-1}$, the relative energy of isomer III is predicted to be -12.4 kcal/mol, showing significant stability compared to isomer I. When the super-atomic 1S and 1P energy levels of the different isomers are compared for this cluster, it is seen that 1S and 1P levels become significantly more stable for isomer III compared to isomer I, similar to the case shown in Figure 4. This is, of course, related to the presence of a central Au atom in the isomer III structure. In fact, the 1S and 1P levels are slightly more stable in the electronic structure of isomer III compared to the case in isomer II. Nevertheless, isomer II is still predicted to be the most stable isomer with a relative energy of -16.2 kcal/mol. This is most likely due to the fact that Au-Ag exchange in the ligand shell results in relatively weaker Ag-S bonds compared to Au-S bond.[70] This is illustrated in the following reaction to model the effect of metal exchange occurring in the ligand shell doping in the isomer III structure:

$$Au_2(SH)_3^{-1} + Ag^{+1} \rightarrow AgAu(SH)_3^{-1} + Au^{+1} \quad (1)$$

The ΔE of this reaction is calculated to be ~20 kcal/mol favoring the reactant side as $Au_2(SH)_3^{-1}$ is predicted to be energetically more favorable compared to $AgAu(SH)_3^{-1}$. This result agrees with our prediction for the relative stability of isomer III in $AgAu_{24}^{-1}$. We also expect that the relative stability of isomer III will mainly be determined by the competition between the more stable Au_{13} core and less stable RS-M-SR bonds when compared to the isomer I or isomer II structures for other dopants.

CONCLUSIONS

We have investigated the geometries, relative energies and electronic structure for different isomers of doped MAu_{24}, MAg_{24} and MAu_{37} systems. For the geometries of MAu_{24} and MAg_{24}, our results show that the metallic radii of the dopant can affect the overall geometry of the cluster. There is a good linear correlation between M-Au or M-Ag bond lengths and the metallic radii of the dopant for isomer I and isomer II structures. One main difference is that the bond-length variation is significantly larger in the isomer II structure compared to the isomer I case as a result of symmetry. This result also agrees with the calculated reorganization energies (ΔE_{reorg}) of the doped cluster. We also note that the energy separation between the two isomers becomes larger when the geometry is relaxed as ΔE_{reorg} energies are considerably larger for isomer II.

While the geometry of the doped cluster shows some dependence on the nature of the dopant, the relative isomer energies are found to be mostly determined by electronic effects introduced by doping. This is most obvious in Ag doped MAu_{24} and MAu_{37} as well as Au doped MAg_{24} where the geometry of the doped cluster is quite similar to the parent undoped cluster. For group X dopants (Ni, Pd and Pt), the isomer I geometry is favored significantly for all investigated systems due to the interactions between the nd levels that originate from the dopant and the super-atomic levels. As one moves right across the periodic table from group X, the couplings between nd levels and super-atomic levels become smaller, and they do not play an important role in the relative stabilities of isomers.

In the case of MAu_{24} and MAu_{37}, there is an energy penalty when the central Au atom in the core is replaced by group XI, XII and XIII dopants. As a result, isomer II is predicted to be more stable compared to isomer I for these dopants. The relative isomer energies also correlate with the energies of the 1P and 1S levels in these isomers. This energy penalty can be explained by the larger s and p contributions of the central atom in isomer I as a result of symmetry considerations, and the large relativistic stabilization of the s and p levels in the case of Au. In general, our results show that will be quite unlikely to obtain the isomer I structure in MAu_{24} and MAu_{37} for dopants that are on the right-hand side of group X, as isomer II or isomer III structures are favored for these systems.

In the case of MAg_{24}, relative isomer energies show significant differences compared to MAu_{24}. In general, there is a shift for the calculated energy separation between isomer I and isomer II in favor of the isomer I structure for the silver-based system. Additionally, 1P and 1S levels are generally more stable in the isomer I electronic structure, unlike the case in MAu_{24}. This is, of course, related to the fact that the relativistic stabilization for the s and p levels of Ag is much smaller compared to the case in Au, and there is not a large energy penalty when replacing the central Ag with a dopant. In this case, our results show that it is possible to yield a thermodynamically preferred isomer I for dopants that are on the right-hand side of group X.

Conflict of Interest

There are no conflicts to declare.

Supporting Information

The possible unique positions for dopants in the MAu_{37} cluster, discussion of fragment calculations for the Mulliken population analysis of MOs, tabulated MO population analysis for selected systems, tabulated Mulliken charges and partial populations for MAu_{24}, MAg_{24} and MAu_{37} systems, comparison of atomic energy levels in Cu^{+1}, Ag^{+1} and Au^{+1}, the correlation between

metallic radii and M-Ag bonds in MAg_{24}, and relative isomer energies and HOMO-LUMO gaps for isomer III structures of MAu_{24} and MAg_{24}.

Acknowledgements

This material is based on work supported by the National Science Foundation under Grant CHE-1507909. The computing for this project was performed on the Beocat Research Cluster at Kansas State University, which is funded in part by NSF grants CHE-1726332, CNS-1006860, EPS-1006860, and EPS-0919443. The authors thank Prof. Chris Ackerson and Prof. Ken Knappenberger for interesting discussions regarding doped nanocluster synthesis.

REFERENCES

1. Akola, J.; Walter, M.; Whetten, R. L.; Hakkinen, H.; Groenbeck, H. On the Structure of Thiolate-Protected Au_{25}. *J. Am. Chem. Soc.* **2008**, *130*, 3756-3757.
2. Hakkinen, H. Atomic and Electronic Structure of Gold Clusters: Understanding Flakes, Cages and Superatoms from Simple Concepts. *Chem. Soc. Rev.* **2008**, *37*, 1847-1859.
3. Heaven, M. W.; Dass, A.; White, P. S.; Holt, K. M.; Murray, R. W. Crystal Structure of the Gold Nanoparticle $N(C_8H_{17})_4$ $Au_{25}(SCH_2CH_2Ph)_{18}$. *J. Am. Chem. Soc.* **2008**, *130*, 3754-3755.
4. Walter, M.; Akola, J.; Lopez-Acevedo, O.; Jadzinsky, P. D.; Calero, G.; Ackerson, C. J.; Whetten, R. L.; Gronbeck, H.; Hakkinen, H. A Unified View of Ligand-Protected Gold Clusters as Superatom Complexes. *Proc. Natl. Acad. Sci. U.S.A.* **2008**, *105*, 9157-9162.
5. Zhu, M.; Aikens, C. M.; Hollander, F. J.; Schatz, G. C.; Jin, R. Correlating the Crystal Structure of a Thiol-Protected Au_{25} Cluster and Optical Properties. *J. Am. Chem. Soc.* **2008**, *130*, 5883-5885.
6. Jin, R. C.; Zeng, C. J.; Zhou, M.; Chen, Y. X. Atomically Precise Colloidal Metal Nanoclusters and Nanoparticles: Fundamentals and Opportunities. *Chem. Rev.* **2016**, *116*, 10346-10413.
7. Chakraborty, I.; Pradeep, T. Atomically Precise Clusters of Noble Metals: Emerging Link between Atoms and Nanoparticles. *Chem. Rev.* **2017**, *117*, 8208-8271.
8. Jadzinsky, P. D.; Calero, G.; Ackerson, C. J.; Bushnell, D. A.; Kornberg, R. D. Structure of a Thiol Monolayer-Protected Gold Nanoparticle at 1.1 Angstrom Resolution. *Science* **2007**, *318*, 430-433.
9. Qian, H.; Jiang, D.-e.; Li, G.; Gayathri, C.; Das, A.; Gil, R. R.; Jin, R. Monoplatinum Doping of Gold Nanoclusters and Catalytic Application. *J. Am. Chem. Soc.* **2012**, *134*, 16159-16162.
10. Stratakis, M.; Garcia, H. Catalysis by Supported Gold Nanoparticles: Beyond Aerobic Oxidative Processes. *Chem. Rev.* **2012**, *112*, 4469-4506.
11. Xie, S.; Tsunoyama, H.; Kurashige, W.; Negishi, Y.; Tsukuda, T. Enhancement in Aerobic Alcohol Oxidation Catalysis of Au_{25} Clusters by Single Pd Atom Doping. *ACS Catal.* **2012**, *2*, 1519-1523.
12. Yu, C. L.; Li, G.; Kumar, S.; Kawasaki, H.; Jin, R. C. Stable $Au_{25}(SR)_{18}/TiO_2$ Composite Nanostructure with Enhanced Visible Light Photocatalytic Activity. *J. Phys. Chem. Lett.* **2013**, *4*, 2847-2852.
13. Zhu, Y.; Qian, H.; Jin, R. Catalysis Opportunities of Atomically Precise Gold Nanoclusters. *J. Mater. Chem.* **2011**, *21*, 6793-6799.
14. Zhang, Y.; Chu, W.; Foroushani, A. D.; Wang, H.; Li, D.; Liu, J.; Barrow, C. J.; Wang, X.; Yang, W. New Gold Nanostructures for Sensor Applications: A Review. *Materials* **2014**, *7*, 5169-5201.
15. Yang, X.; Yang, M.; Pang, B.; Vara, M.; Xia, Y. Gold Nanomaterials at Work in Biomedicine. *Chem. Rev.* **2015**, *115*, 10410-10488.
16. Chen, Y. S.; Choi, H.; Kamat, P. V. Metal-Cluster-Sensitized Solar Cells. A New Class of Thiolated Gold Sensitizers Delivering Efficiency Greater Than 2%. *J. Am. Chem. Soc.* **2013**, *135*, 8822-8825.
17. Hakkinen, H.; Walter, M.; Gronbeck, H. Divide and Protect: Capping Gold Nanoclusters with Molecular Gold-Thiolate Rings. *J. Phys. Chem. B* **2006**, *110*, 9927-9931.
18. Qian, H. F.; Eckenhoff, W. T.; Zhu, Y.; Pintauer, T.; Jin, R. C. Total Structure Determination of Thiolate-Protected Au_{38} Nanoparticles. *J. Am. Chem. Soc.* **2010**, *132*, 8280-8281.

19. Das, A.; Liu, C.; Byun, H. Y.; Nobusada, K.; Zhao, S.; Rosi, N.; Jin, R. C. Structure Determination of $Au_{18}(SR)_{14}$. *Angew. Chem. Int. Ed.* **2015**, *54*, 3140-3144.
20. Crasto, D.; Malola, S.; Brosofsky, G.; Dass, A.; Hakkinen, H. Single Crystal XRD Structure and Theoretical Analysis of the Chiral $Au_{30}S(S\text{-}t\text{-}Bu)_{18}$ Cluster. *J. Am. Chem. Soc.* **2014**, *136*, 5000-5005.
21. Zeng, C. J.; Chen, Y. X.; Iida, K.; Nobusada, K.; Kirschbaum, K.; Lambright, K. J.; Jin, R. C. Gold Quantum Boxes: On the Periodicities and the Quantum Confinement in the Au_{28}, Au_{36}, Au_{44}, and Au_{52} Magic Series. *J. Am. Chem. Soc.* **2016**, *138*, 3950-3953.
22. Chen, Y. X.; Zeng, C. J.; Liu, C.; Kirschbaum, K.; Gayathri, C.; Gil, R. R.; Rosi, N. L.; Jin, R. C. Crystal Structure of Barrel-Shaped Chiral $Au_{130}(P\text{-}MBT)_{50}$ Nanocluster. *J. Am. Chem. Soc.* **2015**, *137*, 10076-10079.
23. Jin, R. X.; Zhao, S.; Xing, Y.; Jin, R. C. All-Thiolate-Protected Silver and Silver-Rich Alloy Nanoclusters with Atomic Precision: Stable Sizes, Structural Characterization and Optical Properties. *CrystEngComm* **2016**, *18*, 3996-4005.
24. Joshi, C. P.; Bootharaju, M. S.; Alhilaly, M. J.; Bakr, O. M. $Ag_{25}(SR)_{18}$: The "Golden" Silver Nanoparticle. *J. Am. Chem. Soc.* **2015**, *137*, 11578-11581.
25. Yang, H.; Wang, Y.; Huang, H.; Gell, L.; Lehtovaara, L.; Malola, S.; Hakkinen, H.; Zheng, N. All-Thiol-Stabilized Ag_{44} and $Au_{12}ag_{32}$ Nanoparticles with Single-Crystal Structures. *Nat. Commun.* **2013**, *4*, 2422.
26. Kang, X.; Chong, H. B.; Zhu, M. Z. $Au_{25}(SR)_{18}$: The Captain of the Great Nanocluster Ship. *Nanoscale* **2018**, *10*, 10758-10834.
27. Lopez-Acevedo, O.; Tsunoyama, H.; Tsukuda, T.; Hakkinen, H.; Aikens, C. M. Chirality and Electronic Structure of the Thiolate-Protected Au_{38} Nanocluster. *J. Am. Chem. Soc.* **2010**, *132*, 8210-8218.
28. Jin, R. C. Atomically Precise Metal Nanoclusters: Stable Sizes and Optical Properties. *Nanoscale* **2015**, *7*, 1549-1565.
29. Weerawardene, K.; Hakkinen, H.; Aikens, C. M. In *Annual Review of Physical Chemistry*, Johnson, M. A.; Martinez, T. J. Eds. 2018; Vol. 69, pp 205-229.
30. Castleman, A. W.; Khanna, S. N. Clusters, Superatoms, and Building Blocks of New Materials. *J. Phys. Chem. C* **2009**, *113*, 2664-2675.
31. Bergeron, D. E.; Roach, P. J.; Castleman, A. W.; Jones, N.; Khanna, S. N. Al Cluster Superatoms as Halogens in Polyhalides and as Alkaline Earths in Iodide Salts. *Science* **2005**, *307*, 231-235.
32. Zhu, M.; Aikens, C. M.; Hendrich, M. P.; Gupta, R.; Qian, H.; Schatz, G. C.; Jin, R. Reversible Switching of Magnetism in Thiolate-Protected Au_{25} Superatoms. *J. Am. Chem. Soc.* **2009**, *131*, 2490-2492.
33. Cheng, L. J.; Ren, C. D.; Zhang, X. Z.; Yang, J. L. New Insight into the Electronic Shell of $Au_{38}(SR)_{24}$: A Superatomic Molecule. *Nanoscale* **2013**, *5*, 1475-1478.
34. Fields-Zinna, C. A.; Crowe, M. C.; Dass, A.; Weaver, J. E. F.; Murray, R. W. Mass Spectrometry of Small Bimetal Monolayer-Protected Clusters. *Langmuir* **2009**, *25*, 7704-7710.
35. Jiang, D. E.; Dai, S. From Superatomic $Au_{25}(SR)_{18}^{-}$ to Superatomic $M@Au_{24}(SR)_{18}^{q}$ Core-Shell Clusters. *Inorg. Chem.* **2009**, *48*, 2720-2722.
36. Walter, M.; Moseler, M. Ligand-Protected Gold Alloy Clusters: Doping the Superatom. *J. Phys. Chem. C* **2009**, *113*, 15834-15837.
37. Kumara, C.; Aikens, C. M.; Dass, A. X-Ray Crystal Structure and Theoretical Analysis of $Au_{25\text{-}X}Ag_X(SCH_2CH_2Ph)_{18}^{-}$ Alloy. *J. Phys. Chem. Lett.* **2014**, *5*, 461-466.

38. Yamazoe, S.; Kurashige, W.; Nobusada, K.; Negishi, Y.; Tsukuda, T. Preferential Location of Coinage Metal Dopants (M = Ag or Cu) in $Au_{25-X}M_X(SC_2H_4Ph)_{18}^-$ (X ~ 1) as Determined by Extended X-Ray Absorption Fine Structure and Density Functional Theory Calculations. *J. Phys. Chem. C* **2014**, *118*, 25284-25290.
39. Yao, C.; Chen, J.; Li, M.-B.; Liu, L.; Yang, J.; Wu, Z. Adding Two Active Silver Atoms on Au_{25} Nanoparticle. *Nano Lett.* **2015**, *15*, 1281-1287.
40. Yao, C.; Lin, Y.-j.; Yuan, J.; Liao, L.; Zhu, M.; Weng, L.-h.; Yang, J.; Wu, Z. Mono-Cadmium Vs Mono-Mercury Doping of Au_{25} Nanoclusters. *J. Am. Chem. Soc.* **2015**, *137*, 15350-15353.
41. Negishi, Y.; Kurashige, W.; Niihori, Y.; Iwasa, T.; Nobusada, K. Isolation, Structure, and Stability of a Dodecanethiolate-Protected Pd_1Au_{24} Cluster. *Phys. Chem. Chem. Phys.* **2010**, *12*, 6219-6225.
42. Christensen, S. L.; MacDonald, M. A.; Chatt, A.; Zhang, P.; Qian, H. F.; Jin, R. C. Dopant Location, Local Structure, and Electronic Properties of $Au_{24}Pt(SR)_{18}$ Nanoclusters. *J. Phys. Chem. C* **2012**, *116*, 26932-26937.
43. Negishi, Y.; Kurashige, W.; Kobayashi, Y.; Yamazoe, S.; Kojima, N.; Seto, M.; Tsukuda, T. Formation of a $Pd@Au_{12}$ Superatomic Core in $Au_{24}Pd_1(SC_{12}H_{25})_{18}$ Probed by Au^{197} Mossbauer and Pd K-Edge EXAFS Spectroscopy. *J. Phys. Chem. Lett.* **2013**, *4*, 3579-3583.
44. Kwak, K.; Tang, Q.; Kim, M.; Jiang, D.-e.; Lee, D. Interconversion between Superatomic 6-Electron and 8-Electron Configurations of $M@Au_{24}(SR)_{18}$ Clusters (M = Pd, Pt). *J. Am. Chem. Soc.* **2015**, *137*, 10833-10840.
45. Tian, S. B.; Liao, L. W.; Yuan, J. Y.; Yao, C. H.; Chen, J. S.; Yang, J. L.; Wu, Z. K. Structures and Magnetism of Mono-Palladium and Mono-Platinum Doped $Au_{25}(PET)_{18}$ Nanoclusters. *Chem. Commun.* **2016**, *52*, 9873-9876.
46. Tofanelli, M. A.; Ni, T. W.; Phillips, B. D.; Ackerson, C. J. Crystal Structure of the $PdAu_{24}SR_{18}^0$ Superatom. *Inorg. Chem.* **2016**, *55*, 999-1001.
47. Bhat, S.; Baksi, A.; Mudedla, S. K.; Natarajan, G.; Subramanian, V.; Pradeep, T. $Au_{22}Ir_3(PET)_{18}$: An Unusual Alloy Cluster through Intercluster Reaction. *J. Phys. Chem. Lett.* **2017**, *8*, 2787–2793.
48. Yan, J.; Su, H.; Yang, H.; Malola, S.; Lin, S.; Haekkinen, H.; Zheng, N. Total Structure and Electronic Structure Analysis of Doped Thiolated Silver $MAg_{24}(SR)_{18}^{2-}$ (M = Pd, Pt) Clusters. *J. Am. Chem. Soc.* **2015**, *137*, 11880-11883.
49. Bootharaju, M. S.; Joshi, C. P.; Parida, M. R.; Mohammed, O. F.; Bakr, O. M. Templated Atom-Precise Galvanic Synthesis and Structure Elucidation of a $Ag_{24}Au(SR)_{18}^-$ Nanocluster. *Angew. Chem. Int. Ed.* **2016**, *55*, 922-926.
50. Liu, X.; Yuan, J. Y.; Yao, C. H.; Chen, J. S.; Li, L. L.; Bao, X. L.; Yang, J. L.; Wu, Z. K. Crystal and Solution Photoluminescence of $MAg_{24}(SR)_{18}$ (M = Ag/Pd/Pt/Au) Nanoclusters and Some Implications for the Photoluminescence Mechanisms. *J. Phys. Chem. C* **2017**, *121*, 13848-13853.
51. Negishi, Y.; Igarashi, K.; Munakata, K.; Ohgake, W.; Nobusada, K. Palladium Doping of Magic Gold Cluster $Au_{38}(SC_2H_4Ph)_{24}$: Formation of $Pd_2Au_{36}(SC_2H_4Ph)_{24}$ with Higher Stability Than $Au_{38}(SC_2H_4Ph)_{24}$. *Chem. Commun.* **2012**, *48*, 660-662.
52. Barrabes, N.; Zhang, B.; Burgi, T. Racemization of Chiral $Pd_2Au_{36}(SC_2H_4Ph)_{24}$: Doping Increases the Flexibility of the Cluster Surface. *J. Am. Chem. Soc.* **2014**, *136*, 14361-14364.
53. Kumara, C.; Gagnon, K. J.; Dass, A. X-Ray Crystal Structure of $Au_{38-X}Ag_X(SCH_2CH_2Ph)_{24}$ Alloy Nanomolecules. *J. Phys. Chem. Lett.* **2015**, *6*, 1223-1228.

54. Zhang, B.; Kaziz, S.; Li, H.; Wodka, D.; Malola, S.; Safonova, O.; Nachtegaal, M.; Mazet, C.; Dolamic, I.; Llorca, J.; et al. $Pd_2Au_{36}(SR)_{24}$ Cluster: Structure Studies. *Nanoscale* **2015**, *7*, 17012-17019.
55. Zhang, B.; Burgi, T. Doping Silver Increases the $Au_{38}(SR)_{24}$ Cluster Surface Flexibility. *J. Phys. Chem. C* **2016**, *120*, 4660-4666.
56. Kim, M.; Tang, Q.; Kumar, A. V. N.; Kwak, K.; Choi, W.; Jiang, D. E.; Lee, D. Dopant-Dependent Electronic Structures Observed for $M_2Au_{36}(SC_6H_{13})_{24}$ Clusters (M = Pt, Pd). *J. Phys. Chem. Lett.* **2018**, *9*, 982-989.
57. Liao, L. W.; Zhou, S. M.; Dai, Y. F.; Liu, L. R.; Yao, C. H.; Fu, C. F.; Yang, J. L.; Wu, Z. K. Mono-Mercury Doping of Au_{25} and the HOMO/LUMO Energies Evaluation Employing Differential Pulse Voltammetry. *J. Am. Chem. Soc.* **2015**, *137*, 9511-9514.
58. Alkan, F.; Munoz-Castro, A.; Aikens, C. M. Relativistic DFT Investigation of Electronic Structure Effects Arising from Doping the Au_{25} Nanocluster with Transition Metals. *Nanoscale* **2017**, *9*, I15825-15834.
59. Perdew, J. P.; Burke, K.; Ernzerhof, M. Generalized Gradient Approximation Made Simple. *Phys. Rev. Lett.* **1996**, *77*, 3865-3868.
60. Perdew, J. P.; Burke, K.; Wang, Y. Generalized Gradient Approximation for the Exchange-Correlation Hole of a Many-Electron System. *Phys. Rev. B* **1996**, *54*, 16533-16539.
61. Lenthe, E. v.; Baerends, E. J.; Snijders, J. G. Relativistic Total Energy Using Regular Approximations. *J. Chem. Phys.* **1994**, *101*, 9783-9792.
62. Lenthe, E. v.; Snijders, J. G.; Baerends, E. J. The Zero-Order Regular Approximation for Relativistic Effects: The Effect of Spin--Orbit Coupling in Closed Shell Molecules. *J. Chem. Phys.* **1996**, *105*, 6505-6516.
63. van Lenthe, E.; van Leeuwen, R.; Baerends, E. J.; Snijders, J. G. Relativistic Regular Two-Component Hamiltonians. *Int. J. Quantum Chem.* **1996**, *57*, 281-293.
64. ADF2017, *SCM, Theoretical Chemistry, Vrije Universiteit, Amsterdam, The Netherlands,* http://www.scm.com/ (accessed Jan 1, 2017).
65. Guerra, C. F.; Snijders, J. G.; te Velde, G.; Baerends, E. J. Towards an Order-N DFT Method. *Theor. Chem. Acc.* **1998**, *99*, 391-403.
66. te Velde, G.; Bickelhaupt, F. M.; Baerends, E. J.; Guerra, C. F.; Van Gisbergen, S. J. A.; Snijders, J. G.; Ziegler, T. Chemistry with ADF. *J. Comput. Chem.* **2001**, *22*, 931-967.
67. Greenwood, N. N.; Earnshaw, A. *Chemistry of the Elements*; Elsevier: Amsterdam, 1997.
68. Pyykko, P. Relativistic Effects in Structural Chemistry. *Chem. Rev.* **1988**, *88*, 563-594.
69. Autschbach, J. Perspective: Relativistic Effects. *J. Chem. Phys.* **2012**, *136*, 150902.
70. Pakiari, A. H.; Jamshidi, Z. Nature and Strength of M-S Bonds (M = Au, Ag, and Cu) in Binary Alloy Gold Clusters. *J. Phys. Chem. A* **2010**, *114*, 9212-9221.

TOC graphic